Study of the permeability in the Opalinus clay series (Mont Terri -Switzerland) using the steady state method in Hassler cell

Stéphane Al Reda, Catherine Yu, Guillaume Berthe, Jean-Michel Matray

Study of the permeability in the Opalinus clay series (Mont Terri -Switzerland) using the steady state method in Hassler cell

Stéphane M. Al Reda,, Catherine Yu, Guillaume Berthe, Jean-Michel Matray

GEOPS, Univ. Paris Sud, CNRS, Universit? Paris-Saclay, 91405, Orsay, Cedex, France
Institut de Radioprotection et de S?ret? Nucl?aire, 31 Allée du Général Leclerc, F92260, Fontenay-aux-Roses, France
IFP Energie nouvelles, 1-4 Avenue du Bois Préau, 92852, Rueil Malmaison, France

A B S T R A C T

The Mont Terri rock laboratory located in the Northwestern Switzerland is an international platform for applied research in the field of radioactive waste disposal in clayrock formations. A borehole named BDB1 has been drilled in the Opalinus claystone in 2013 to assess its containment properties. Characterization of petrophysical and hydrogeological parameters in the Jurassic shale known as Opalinus Clay were performed by in situ experiments conducted in the rock laboratory of Jura Mountains and on borehole samples. This paper presents the results of laboratory measurements of permeability in a permeameter called Hassler cell by using the steady state method. The study is applied to core samples drilled perpendicular and parallel to the bedding, and involves gas and water permeability measurements. The Hassler cell is an experimental device that allows to put samples under a confining pressure reproducing the in situ one. In all, results were obtained for nine samples over sixteen for gas permeability measurements with values ranging between 6.9×10^{-21} and 2.3×10^{-19}m2 and one sample for water permeability measurements with a value of 1.38×10^{-20}m2. Most of the results are in good agreement with previous studies obtained by in situ experiments and using the Poiseuille type law method. The usage of several methods to determine the permeability of the Opalinus clay unit helps to conclude about the accuracy, trueness and precision of the measurements.

Keywords : Mont Terri, Opalinus clay, BDB-1 borehole, Gas permeability, Water permeability, Steady state method, Hassler cell, Slippage effect

1. Introduction:

Considerable researches have been dedicated to the investigations of deep repositories for the storage of radioactive waste in geological formations since 1957. In countries where nuclear power is generated, various types of rock have been studied in order to identify the most convenient material for storage of nuclear wastes. When the host rock for a nuclear waste repository represents the major and final barrier for radionuclides, the repository performance largely relies on its confinement properties. Clay formations have been chosen by France (Callovo-Oxfordian) and Switzerland (Opalinus Clay) to dispose their high-level and long-lived intermediate radioactive waste. Clay rocks exhibit several properties including low permeability and high retention capacity for radionuclides and other contaminants. Understanding the transport mechanisms of the radionuclides is of utmost importance for assessing the safety performance of nuclear waste repositories. Various studies have been conducted on low-permeability clay formations (Ce et al. 2001; Gautschi 2001; Marschall, et al. 2005; Nussbaum et al. 2011; Davy et al. 2013; Cuss et al. 2014; Takeda et al. 2014) in order to understand their hydrogeological and petrophysical properties.

The Opalinus Clay formation has been studied at the security gallery of the A16 Transjurane highway, built in the Jura Mountains in the Northwestern Switzerland. This Mont Terri facility is devoted to the study of the confinement properties of this over-consolidated clay rock. Several geological, geochemical, geomechanical, and hydrogeological studies have been published since 1996 (Thury and Bossart 1999; Marschall et al. 2004; Marschall et al. 2005; Bossart and Milnes 2017). The aim of the current study attached to the DB experiment (Deep Borehole experiment) is to determine the permeability of the Opalinus Clay formation using the steady state method in a Hassler cell and to discuss the new results in light of previous studies. The so-called Hassler cell allows to reproduce the confining pressure of samples (in situ stress pressure) and to determine the gas and water permeability. The steady state method

consists in applying a pressure gradient over a sample and measuring the gas flow across it. Gas-driven permeability measurements using this method have the advantage of being quickly performed, they do not contaminate or affect the sample and the analysis of data is simple (Filomena et al., 2014; Singh and Cai, 2019). The acquired measurements are compared to results obtained using a Poiseuille-type law method from previous study (Yu et al., 2017), applied in samples where the flow orientation is parallel to bedding planes. The latter method requires the knowledge of the rock mineralogy and the acquisition of petrophysical parameters such as the water-loss porosity, specific surface area, and grain density. Nevertheless, it requires the usage of a cementation factor of which the estimation is debatable and unclear. In addition, permeability measurements were performed by Yu et al. (2017) using two in situ tests: the pulse withdrawal test and the constant rate withdrawal test applied at a large scale. These two kinds of tests give high ranges of uncertainties. The results obtained using the steady state method in Hassler cell are compared and discussed with permeability values acquired using in situ test and the Poiseuille-type law method.

2. Geological settings

The Dogger unit of the Mont Terri facility comprises several shallowing-upward regressive cycles, starting with Toarcian-Aalenian Opalinus Clay and ending with shallow-water carbonates (Blaesi 1987). The Opalinus Clay (Figure 1) was deposited around 174 Ma ago, and consists of a monotonous sequence of dark grey, silty clays and sandy shales overlain by 800 m of sandy limestone, marls and shales of Middle to Late Jurassic age (Blaesi 1991). A 400 m of Early Jurassic to Triassic marls and limestones, dolomites and anhydrites underlie the clay formation, which has a thickness of 160 m and a true thickness around 90 m. The name of the Opalinus Clay comes from the frequent occurrence of the fossil ammonite *Leioceras opalinum* whose aragonite shell presents opalescent effects.

A period of marine regression between the mid- to late-Cretaceous and the mid-Tertiary

Oligocene period (100-25 Ma) induced a subaerially exposure of the top of the Malm Limestone (Figure 1). Starting about 40 million years ago, the rifting of the Rhine Graben affected Northern Switzerland, resulting in a considerable uplift of the area in the mid-Tertiary, and was followed by down warping and burial under late Tertiary sediments. The Opalinus Clay formation reached a burial depth of 1000 m and 1700 m, respectively during these two phases of subsidence. During the late Miocene to Pliocene stages of the upper Tertiary period (10-2 Ma), the late Alpine folding formed the Folded Jura. Uplift and erosion during the Tertiary and Quaternary periods initiated the influx of meteoric water into the sequence. Towards the end of the Pliocene period (about 2.5 Ma), erosion exposed the core of the Mont Terri anticline to fresh water infiltration into the Dogger limestones. During the Quaternary period, infiltration into the Liassic limestones started, about 350 thousand years ago (Pearson et al. 2003).

Observed minerals in the Opalinus Clay formation are quartz, illite and mixed-layer illite–smectites, kaolinite, chlorite, biotite and muscovite, calcite, aragonite, siderite, dolomite and/or ankerite, albite and/or plagioclase, K-feldspar, pyrite, organic matter, and other accessory minerals such as apatite, celestine, zircon, and monazite (Bossart et al. 2017, 2018). The Opalinus Clay can be divided into five lithostratigraphic sub-units (Schaeren and Norbert 1989; Blaesi 1991; Thury and Bossart 1999; Bossart 2008), which are grouped in three main facies: a shaly facies in the lower part of the sequence, a thin carbonate-rich sandy facies in the middle part of the formation, and a sandy facies interstratified with shaly facies in the upper sequence. The shaly facies contains argillaceous shale (illite, chlorite, kaolinite, and illite-smectite mixed layers) and marly shales with micas and bioturbated layers. Their mineral composition includes 27-78 % of clay minerals, 4-29 % of carbonates, 10-32 % of quartz, and accessory minerals such as feldspar and pyrite (Bossart and Thury, 2008; Schaeren & Norbert, 1989). The sandy facies consists of marly shales with sandstones, limestone layers and pyrites, and the carbonate-rich sandy facies contains calcareous sandstones with bioturbated limestones. These three facies

have been described in detail by Blaesi (1987), Allia (1996), Burkhalter (1996), Burkhalter, et al. (1997). They can be explained by varying sedimentary environments in a shallow coastal basin during the time of deposition.

3. Material and methods

3.1 Core sampling from BDB-1 borehole

"The Deep Borehole Experiement" is a project launched by Swiss, French, Canadian, and German Mont Terri partners in 2015. The main goal of this project is to compare the convective and diffusive transport phenomena within the Opalinus Clay formation and out of the hydraulically-disturbed zone. In order to evaluate the transport properties and processes that affect the Opalinus Clay formation, the deep borehole BDB-1 was drilled normally to the bedding to minimize breakouts at the borehole wall with a 45° downward inclination and completed at a final depth of 247.5 m long. The borehole was entirely cored for stratigraphic, petrophysical, mineralogical, and geochemical studies and was drilled with air as drilling fluid. The stratigraphic sequence crossed by the borehole is described in detail by Jaeggi et al. (2017).

For this study, we used 18 cylindrical Opalinus Clay plugs from the shaly and sandy facies of the borehole. Plugs were drilled normal and parallel to the bedding and standardized to a size of about 40 mm diameter (except sample M21b, Table 1) and variable lengths. The dataset presented in Table 1 shows the name of each sample, its distance from the borehole head, the drilling direction with respect to the bedding, and its size. Prior to permeability measurements, samples were oven-dried at 105 °C until reaching a constant weight (generally achieved in 6 to 10 hours). The brittle behaviour of the Opalinus Clay formation led to some sample cracking due to: i) the high stress applied during drill-core sampling, ii) the unloading during core retrieve, and mainly iii) the drying process. Therefore, a liquid epoxy resin was used to fill the sample voids in order to solve the micro-cracking issues that could bias the permeability results.

Four samples covered with resin were chosen for micro computed tomography analysis M12a, M12d, M13b, and M14c) using Bruker Skyscan 1173, to test the influence of filling the micro-cracks by the resin. The sample M12a is drilled perpendicular to the bedding while the other three samples are drilled parallel to the bedding. The choice of the samples is made according to their degree of damage. The most damaged sample perpendicular to the bedding is choose for analysis.

3.2 Steady state method in a Hassler Cell

Despite the popularity of the unsteady state methods (pulse decay method, oscillating pressure…) and the short time needed for measurements, they remain very complicated in terms of data interpretation and very expensive. The steady state method used here is preferred according to Boulin et al. (2012) for very low permeability porous media such as clays, and give more reliable results, especially when having an appropriate set-up. A brief description of measurement techniques for permeability in shale, is available in Singh and Cai (2019) with their corresponding advantages and inconveniences. The simple setup and analysis of data using Darcy's law expression in the steady state method are the main advantages that encourage the using of this technique. Moreover, the interpretation of the acquired data is less complicated compared to unsteady state methods and are not sensitive to temperature fluctuations, porosity and system volume (Singh and Cai 2019b). The time of water permeability measurements in Hassler cell using the steady state method depends mainly on the time needed to saturate the sample, that is significantly long in this study compared to the gas permeability measurements using the same method.

Hassler type core holders are defined as core holders that have isotropic confining pressure applied to the core sample. A Hassler cell is a cylindrical standard laboratory device used to measure water and gas permeability of a core sample. A Hassler cell containing a clay sample is presented in Figure 2A. Manometers *P1, P2,* and *P3* are used to measure the applied upstream

pressure (P_u), the received downstream pressure (P_d), and the confining pressure P_{conf} (black arrows in Figure 2A) respectively. The upstream pressure is kept constant by a Brooks® pressure regulator and the flowrate is measured by a Brooks® flowmeter. The direct and accurate reading of flowrates makes the steady state method potentially faster for clay samples than the pulse decay method (Boulin et al., 2012). It consists of imposing a differential pressure *(*$DP = P_u - P_d$*)* over a sample and measuring the flowrate at the outflow.

The graphs of Figure 2 show the response registered by manometers after imposing a pressure to saturate the plug with nitrogen gas (Figure 2B). Measurements are performed only when the upstream pressure is reached in the downstream side.

3.2.1 Generic procedure

Darcy's law describes the flow induced by a pressure gradient within a porous medium as:

$$q = -\frac{k_f}{\mu_f}.\frac{DP}{L} \quad (1)$$

Where q is the Darcy velocity (m/s), k_f is the permeability of the porous media (m^2), μ_f is the fluid viscosity (cP), DP is differential pressure (bar) ($DP = P_u - P_d$) and L the length of the sample (cm). The corresponding flowrate Q (m^3/s) is q times S, where S is the sample surface (m^2). We applied multiple pressure gradients respecting the formulae below:

$$P_m = \frac{P_u + P_d}{2} \quad (2)$$

$$P_{eff} = P_{conf} - P_m \quad (3)$$

Where P_m is the mean pressure and P_{eff} is the effective pressure.

3.2.2 Gas permeability measurements

For every gas permeability measurement, the effective pressure was maintained constant and considered to be equal to the extrapolated confinement pressure estimated by the weight of the overlying sediments. When the upstream and downstream pressures change, the confinement pressure changes too according to equation (3). For sample M12a for instance, the extrapolated

confinement pressure was set to 60 bars (6.0 MPa = 870.23 Psi), the upstream and downstream pressures were set to 15 and 5 bars, respectively, and thus the imposed confinement pressure P_{conf} was 70 bars (7 MPa = 1015.26 Psi).

The apparent permeability can be calculated using the following relationship:

$$k_g = 2\frac{\mu.L.Q.P}{S(Pu^2 - Pd^2)} \quad (4)$$

Where k_g is the apparent permeability (can be expressed in m^2 or in mD), μ is the gas viscosity (cP), L is the length of the plug (cm), Q is the flowrate (cm^3/s), P is the measured flow pressure (fixed at 1.022 bar absolute = 1.022 Pa = $1.45.10^{-4}$ Psi), S is the surface of the plug (cm^2), and lastly P_u and P_d respectively represent the upstream and downstream pressures (bar absolute).

Such apparent permeability is overestimated compared to the intrinsic permeability due to the slippage effect (Klinkenberg et al., 1941). Klinkenberg et al., (1941) noted a relationship between mean pore pressure in gas permeability measurements and the mean free path (average distance a gas molecule travels between two successive collisions with other gas molecules) of the flowing gas molecules. A gas slippage occurs when the mean free path of the gas is sufficiently large (meaning that the distance between two successive collisions of gas molecules with each other is long) leading molecules to flow faster in a capillary pore. The resulted permeability is therefore misleading and needs to be corrected (Klinkenberg et al., 1941). Slippage effect is controlled by the imposed pressures and the capillary size. Such relationship has been used by other authors and further described in the studies of McPhee et al. (1994), Filomena et al. (2014), Letham and Bustin (2015). At high pore pressure, molecules are in direct contact with one another (short mean free path), resulting in zero velocity on pore walls (no slippage effect). The slippage effect cannot occur when a gas with small molecular size, and therefore a high mean free path, flows at low pressure (Profice, 2014). Figure 3 shows the slippage effect for capillaries of different geometries and imposed pressures; coloured regions

in grey represent areas at the pore walls where slippage takes place and red colour represents low velocity areas in the inner part of the pore wall . The parameters having an influence on the occurrence of slippage effect are mainly the imposed pressure, the mean free path of the gas, the reflection coefficient (rf) (an approach used by Arabjamaloei and Ruth (2016) defined as the bounce-back effect going in the opposite direction of the flow and leading to a near zero velocity at the pore wall) and the capillary size. The "rf" acts the same way as the pressure and the velocity in the capillary. At very high imposed pressure as in (A), the "rf" is high (E) resulting in a higher velocity at the pore walls. However, the mean free path of the gas (acting in the opposite way of the imposed pressure) is small and the slippage effect do not take place. When the imposed pressure decreases as in (B), the "rf" and the velocity at the pore walls decreases too, resulting in a larger mean free path of the gas and the onset of slippage effect. In (C), the imposed pressure is still decreasing, as same as the "rf" and the velocity at the pore walls, while the mean free path is increasing and the slippage effect is larger. In (B) and (C) the capillary size remain constant. When the capillary size decrease, with keeping the same imposed conditions as in (B), slippage effect appears greater comparing to the capillary size.

In order to correct the apparent permeability for the slippage effect, Klinkenberg et al. (1941) described the relationship between apparent and intrinsic permeabilities as follows:

$$k_g = \beta k_l \frac{1}{P_m} + k_l \qquad (5)$$

Where k_l is the intrinsic permeability and β is Klinkenberg's slippage parameter. According to Klinkenberg et al. (1941), β quantifies how much apparent gas permeability will vary due to slippage at low pressures and is related to the size of the pores in which the gas flows. Klinkenberg plots have been generated by plotting the apparent permeability (calculated using Equation 5) against the inverse of the mean pressure for each pressure gradient and applying a linear fit to the data (Figure 4). The intercept of the linear fit with the permeability axis gives *kl*, the value of the intrinsic permeability, where no slippage takes place.

198

199 3.2.3 Water permeability measurements

200 The steady state method used for water permeability measurements allows a rapid acquisition
201 of the flowrate through a sample in a Hassler cell. The values of the flowrates depend on the
202 pressure gradients imposed on the sample, and they serve to calculate the permeability values.
203 QUIZIX pumps are used in the measurement. They comprise two pistons connected to the
204 upstream and downstream boundaries of the plug, each working independently. The
205 displacement volume in each pump serves to calculate the flowrate through the sample. The
206 pistons move in a push-pull configuration as shown in Figure 5.

207 As in gas permeability measurements, the first step in water permeability measurement
208 consists of saturating the plug. This step took about 15 days for our Opalinus Clay samples.
209 Water with a chemical composition similar to the pore water composition of the sample was
210 used to prevent and limit any potential change in the sample properties (Table 2).
211 Darcy's law described in Equation (1) (section 3.2.1) is used for water permeability
212 measurements. Chosen pressures are based on Equations (2) and (3) with keeping confining,
213 effective, and mean pressures constant; only the upstream and downstream pressures are
214 changed. For example, on sample M12c, parallel to the bedding plane and covered with resin,
215 the upstream pressures were set successively to 80, 90, 100, and 110 bar (8, 9, 10 and 11 MPa
216 = 1160.3, 1305.34, 1450.38 and 1595.42 Psi respectively) , while the corresponding
217 downstream pressures were set respectively to 60, 50, 40, and 30 bar in such a way that the
218 mean pore pressure was maintained at 70 bar (7 MPa = 1015.26 Psi). Once the measurement is
219 finished, we plot the variation of upstream and downstream water volumes during the
220 experiment (Upstream "U" and Downstream "D", working independently and linked to the
221 upstream and the downstream pressures as explained before), as shown in Figure 6.

Water volume in the upstream side of the cell (Upstream, Figure 6) passes through the sample to its downstream side. Figure 6 shows upstream volume decreasing during time and downstream volume increasing (Downstream, Figure 6). We imposed 5 different pressure gradients for each measurement and plotted the corresponding trendlines. The slopes of the equations represent the flowrate (cm^3/s).

Then, we used Darcy's equation to calculate the sample permeability:

$$k = \frac{\mu L Q}{S \Delta P} 1.013 \qquad (6)$$

Where k is the permeability of the sample (mD), μ is the water viscosity (cP), L is the sample length, S is the sample surface (cm^2), Q is the flowrate (cm^3/s), 1.013 is the atmospheric pressure (bar) (room pressure) and ΔP is the pressure gradient (bar).

The water viscosity is temperature dependent. The mean temperature of the measurement and water viscosity are about 25°C and 0.891 cP, respectively. Water viscosity is calculated via the equations below (Mercer et al. 1975):

$$\mu_f = (5.38 + 3.8A - 0.26A^2) \cdot 10^{-3} \qquad (7)$$

$$A = \frac{T - 150}{100} \qquad (8)$$

Where A is the generic cross-sectional area of the porous channel, and T is the temperature of the measurement.

Figure 7 shows the flowrate vs. pressure gradients for both Cylinders U and D. The slopes of the equations represent Q/ΔP, which is used to calculate the permeability of the sample via Darcy's equation.

4. Hassler cell permeability results

Sixteen gas permeability measurements were made (Table 3, Figure 8) of which eight have a

243 big permeability values (around 10^{-17} m^2 = 10.13 µD). Samples coming from the same depth
244 and drilled the same way in respect to the bedding have a significant difference in their
245 permeability values. We decided to analyse a selection of the samples covered with resin, of
246 which some have large permeability values. Four samples (M12a (⊥), M12d (//), M13b (//) and
247 M14c (//)) have been analyses using micro-computed tomography. Results show that the cracks
248 are entirely filled with resin for three samples (M12a, M13b and M14c). Very fine micro-
249 cracks, not filled with the resin, were still observed in the fourth sample (M12d) (Figure 8).
250 However, the used voxel resolution (25.01 µm) is not adapted to clearly reveal the content of
251 very fine cracks in the sample in a clear way. We considered that large permeability values
252 acquired in this study are due to the development of very-fine micro-cracks not filled with resin
253 and caused by drilling and drying processes. As the very fine micro cracks could be mainly due
254 to the excessive heating of the samples at 105 °C, a lower temperature could prevent their
255 production. Samples with large permeability values have therefore been rejected and not
256 considered as representative of the Opalinus Clay formation. Satisfactory results obtained in
257 the Hassler cell vary between $2.3x10^{-19}$ (221 nD) and $6.9x10^{-21}$ m^2 (7nD) for both shaly and
258 sandy facies.

259 No noticeable difference in permeability measurements due to facies change (shaly and sandy
260 facies of Opalinus Clay) can be highlighted in this study. Plugs were drilled in two orientations
261 with respect to the bedding, precisely normal and parallel directions. The purpose of drilling
262 different orientations with respect to the bedding is to measure the permeability anisotropy for
263 the Opalinus Clay formation. However, our results do not allow estimating anisotropy because
264 of the high stress developed during samples preparation and because of their fragility. For water
265 permeability measurements, one result over two is satisfactory. Figure 9 shows gas and water
266 permeability results considered as representative of the Opalinus Clay and acquired in Hassler
267 cell using the steady state method.

5. Comparison of permeability results acquired from different methods

5.1 The Poiseuille-type law method

A petrophysical method based on a semi-empirical Poiseuille type-law has been used by Yu et al. (2017) to calculate the intrinsic permeability of the Opalinus Clay formation. This method was developed and used by Kostek et al. (1992), Pape et al. (1999), and Trémosa (2010) for a flow orientation parallel to the bedding. The model is based on petrophysical parameters: half-pore size (Neuzil 2000; Altinier 2006), formation factor (determined using Archie's law described in Archie, 1952 and also related to diffusion parameters according to Boving & Grathwohl, 2001; Van Loon & Mibus, 2015), porosity, diffusion coefficient in pore water, effective diffusion coefficient, cementation factor, degree of saturation, specific surface area, grain density (obtained by Helium pycnometry), and fluid dynamic viscosity (Mercer et al., 1975).

The intrinsic permeability can be computed using the formula:

$$k = \frac{b^2}{3F} \quad (9)$$

Where k is the intrinsic permeability [m^2], b is the half-pore size [m] and F is the formation factor [-]. The half-pore size can be determined according to the following relation based on a mass balance equation

$$b = \frac{\omega}{(1-\omega)\rho_S A_S} \quad (10)$$

Where ρ_s is the grain density [g m^{-3}], A_s is the specific surface area [m^2 g^{-1}] and ω is the total porosity [-]. Grain density is determined using He pycnometry AccuPyc II 1340 following the protocol described in (Alcade et al., 2013) (see supplementary information for further details). The specific surface area measurement is calculated using the BET method developed by

(Brunauer et al., 1938) by gas adsorption (see supplementary information for further details). Total porosity, ω [-], is the ratio of pore volume V_{pores} [m^3] to total apparent volume V_{tot} [m^3]:

$$\omega = \frac{V_{pores}}{V_{tot}} \quad (11) \qquad V_{pores} = V_{tot} - V_s \quad (12) \qquad V_{pores} = (\pi . r^2 . L) - \frac{M_t}{\rho_s} \quad (13)$$

Where *Vs* is the volume of solids, r is the radius [cm] and L [cm] the length of the sample, M_t [g] is the oven-dried at temperature T=105°C sample mass and ρ_s [$g.cm^{-3}$] is the grain density. The formation factor F accounts for the tortuosity of the porous media and can be determined using the formula

$$F = \omega^{-m} \quad (14)$$

Where m is the cementation factor.

The cementation factor (m) depends on the nature of the porous material. It ranges between 1.3 and 5.4 (Heitzmann 2004), and is estimated to be close to 2 for compacted and deeply buried sediments (Ullman and Aller 1982). For m = 2, the mean intrinsic permeability using semi-empirical Poiseuille-type law is 2.07×10^{-20} m^2 (21 nD) for the Opalinus Clay shaly facies and 2.26×10^{-20} m^2 (23 nD) for its sandy facies (Yu et al. 2017). The intrinsic permeability values acquired using the steady state method in Hassler cell show low variability in results as compared to the values of Poiseuille-type law method. The mean intrinsic permeability using the steady state method is 2.4×10^{-20} m^2 (24 nD) for the shaly facies of the Opalinus Clay formation and 1.15×10^{-19} m^2 (116.6 nD) for its sandy facies. The permeability results acquired using the Poiseuille type-law method are in good agreement with those acquired using the steady state method (Figure 9).

These values are also consistent with the results previously obtained on the Opalinus claystone by gas injection experiments at the Mont Terri rock laboratory or at Benken (North Switzerland)

312 with ranges between $1x10^{-21}$ (10 nD) and $6x10^{-20}$ m^2 (60 nD) (Marschall et al., 2005).

313 5.2 In situ tests method

314 Pulse withdrawal and constant rate withdrawal tests were applied on the sandy and shaly facies
315 of the Opalinus Clay as shown in Figure 9. The permeability results were $2.2x10^{-20}$, $3.2x10^{-20}$
316 m^2 (22, 32 nD) in the sandy facies, and $1.7x10^{-19}$, $2.5x10^{-19}$ m^2 (172, 253 nD) in the shaly facies
317 using the constant rate and the pulse withdrawal tests, respectively. A comparison between the
318 mean permeability results produced by the Hassler cell, Poiseuille-type law, and in situ methods
319 is presented in Table 4. The values ranged from between $2.2x10^{-20}$ (22.3 nD) and $3.2x10^{-20}$ (32.4
320 nD) m^2 for the sandy facies and ranging between $2.21x10^{-20}$ (22.4 nD) and $2.5x10^{-19}$ m^2 (253
321 nD) for the shaly facies. Hassler cell results and in situ tests show the same trend with higher
322 permeability in the shaly facies than in the sandy facies (Table 4).

323 5.3 Acceptance of the results acquired using Hassler cell

324 The micro-computed tomography result of the sample M12d show that very fine micro-cracks
325 in the sample are not filled with resin (it seems that the properties of the resin do not allow the
326 filling of very small voids) (red ellipses in Figure 8A), which explains the very high acquired
327 permeability value (exceeding 10^{-17} m^2 =0.01 mD). Such permeability value is rejected because
328 of the abnormal results compared to those acquired from the same depth. The other three
329 analyzed samples (M12a, M13b and M14c) do not show any very fine micro-cracks and have
330 lower permeabilities. This leads to a first conclusion that the very fine micro-cracks in the
331 sample M12d are responsible of the increasing of the real permeability.
332 As cracks in clay rocks follow the bedding orientation, permeability results of samples drilled
333 perpendicularly to the bedding could be deceptive when covered with resin. The micro-
334 tomography analysis on the sample M12a confirmed that the cracks in such plugs are not
335 blocking gas flow to across the sample from a side to another, and that micro-cracks are mainly

located on the edge. Furthermore, the very close permeability values of the samples M12a (filled with resin) and M12b (non-filled with resin) confirms that the usage of resin do not have any effect the permeability of the sample tested in this study. Although clay formation could contain natural cracks that should be counted in permeability measurements (Singh 2016; Singh and Cai 2019a), very close permeability results of the samples M12a and M12b show that no natural cracks exists in these samples, hence, they have no influence on permeability results. All these reasons are taken into consideration in the acceptance and rejection of permeability results.

Comparing the number of successful measurements for each lithology can provide insight into the reasons why a sample could generate micro-cracks. Precisely, 84 % (five samples out six samples) of the measurements have been successful in the sandy part of the Opalinus Clay formation, and 16 % (one sample, M12d) are rejected because of the micro-cracks. In contrast, 66.6 % of the measurements (4 out of 6) and 50 % (2 out of 4) are rejected in the shaly facies located in the middle of the Opalinus Clay formation and in the latest shaly facies, respectively. As expected, the highest percentage of accepted values is found in the sandy facies, which is less brittle and more resistant to drilling than the shaly facies. The mineralogical composition of each facies of the Opalinus Clay formation can explain such difference (Bossart 2011). The shaly facies located in the middle of the Opalinus Clay formation is mostly composed of silty shale, while the shaly facies (depth between 195 and 235 m) is composed of argillaceous marls (Bossart 2011). Considering the two shaly facies, the observed difference is mainly attributed to the resistance level and rigidity of the rocks, which are partly linked to its composition. Shaly facies contains more clay minerals and less quartz in comparison to the sandy facies (Bossart and Milnes 2017).

Nevertheless, the weakness of the Opalinus Clay formation is not limited to the composition of each facies only. The drilling and drying processes may also have an influence on the generation

of micro-cracks especially in samples drilled parallel to the bedding. The double stress applied on the samples, during the drilling of the borehole BDB-1 and of the plugs for Hassler cell measurement, in addition to the 105°C drying of the Opalinus Clay samples, increases the possibility of cracking and make the acquisition of permeability results very challenging. The use of epoxy resin was the most suitable solution to get a permeability result without any influence on the accuracy of the measurement.

6. Discussion of permeability measurement methods and conclusion

It has been demonstrated in Faulkner and Rutter (2000) that permeability values could vary due to physicochemical interactions between rock and the used fluids. The usage of Argon gas and water in permeability measurements leads to a ~1 order of magnitude difference in results. Layers of strongly adsorbed water on mineral surfaces reduce the effective pore size (Faulkner and Rutter 2000). Each used method has its benefits and inconveniences. The using of several methods is essential to determine the permeability of the Opalinus Clay formation and to minimize the uncertainty of the values. The main advantage of the in situ tests is the possibility to cover a very large surface in the Opalinus Clay formation, which can realize the acquisition of permeability results beyond the borehole damaged zone (also called skin effect). In contrast, the common disadvantages of the laboratory permeability tests (using Poiseuille-type law and Hassler Cell) applied on samples from the BDB-1 borehole are the stress during drilling and the information provided at a smaller scale. Therefore, the satisfaction of a permeability result acquired using permeability tests is only validated after comparison with in situ tests. For the Poiseuille-type law method, the cementation factor choice is debatable and unclear (Yu et al. 2017) (reasons explained in part 5.1), but it establishes results in the same range as in situ tests. The Hassler cell method has the benefit of giving a low range of uncertainties on permeability results compared to the two latter methods but could not be applied for such over consolidated clay without filling stressed plugs with resin. Despite the difference in the solicited volume of

sample between the in situ tests and the laboratory permeability tests, results are rather comparable. The Hassler Cell results did not allow to estimate anisotropy between perpendicular and parallel plugs drilled with respect to the bedding because of the multiple stress induced (drilling and heating). A moderate permeability anisotropy ratio of 5.5, in favour of the permeability parallel to the bedding, was estimated based on laboratory permeameter tests for the Opalinus Clay unit (Croisé et al. 2006). Even though uncertainties on Hassler Cell measurements are quite small, the stress applied to the plugs during drilling makes the steady state method in Hassler Cell not sufficient to give accurate permeability results by itself. In situ hydraulic tests, Poiseuille-type law, and Hassler cell results show similar trends (Figure 8) and give representative values of the Opalinus Clay formation.

The Deep Borehole experiment provided clayrock samples from the hydraulically undisturbed Opalinus Clay formation with the goal of improving the knowledge about its transport properties. A synthesis of the structural and hydrogeological data in the Opalinus Clay formation summarized by Bossart (2011) led to the definition of a 2-meter plastically deformed zone around the drilled zone in the Mont Terri tunnel. This plastic zone is further divided into an inner 1 m zone consisting of an air-filled fracture network and an outer zone with mostly saturated and isolated fractures. In situ hydraulic and permeability data acquired at Mont Terri are or might have been influenced by excavation works and experimental activities and they show high ranges of uncertainties. This study gives a new set of permeability measurements in good agreement with results obtained previously and have accurate ranges of uncertainties (between $1x10^{-31}$ and $1x10^{-33}$ m^2). Microtomography results show that the usage of resin is essential to have accurate values of permeability and to reduce the influence of excavation work generated due to the drilling of the borehole. Gas and water permeability measurements in Hassler Cell, ranging between $1.2.10^{-19}$ (121.6 nD) and $2.58.10^{-20}$ m^2 (26.1 nD) for the sandy facies and between $1.3.10^{-20}$ (13.2 nD) and $6.9.10^{-21}$ m^2 (7 nD) for the shaly facies, are close to

411 the Poiseuille-type law results and in situ tests. Using these three tests allows the acquisition of
412 accurate permeability results representative for the Opalinus Clay formation at large scale.
413 However, the Hassler cell method, devoted to estimate the anisotropy of the samples, does not
414 allow for the determination of the anisotropy for the Opalinus Clay formation due to the high
415 stress applied on samples.
416

Acknowledgments

The authors would like to thank Dr. Janah Shaya for his contribution in the improvement of the English level of this paper.

References

Alcade, G., E. Barker, and S. Bassot. 2013. “Mode Opératoire de la mesure de la surface spécifique d’un solide pulvérulent par adsorption de l’azote par modèle BET.” Document IRSN/PRP-DGE/SRTG/LAME, BET/MOP-01.

Allia, Vincenzo. 1996. *Sedimentologie Und Ablagerungsgeschichte Des Opalinustons in Der Nordschweiz*. na.

Altinier, Maria Victoria. 2006. “Etude de La Composition Isotopique Des Eaux Porales de l’argilite de Tournemire: Inter-Comparaison Des Méthodes de Mesure et Relations Avec Les Paramètres Pétrophysiques.” Paris 11. http://www.theses.fr/2006PA112065.

Arabjamaloei, Rasoul, and Douglas W. Ruth. 2016. “Lattice Boltzmann Based Simulation of Gas Flow Regimes in Low Permeability Porous Media: Klinkenberg’s Region and beyond.” *Journal of Natural Gas Science and Engineering* 31: 405–416.

Archie, Gustave Erdman. 1952. “Classification of Carbonate Reservoir Rocks and Petrophysical Considerations.” *Aapg Bulletin* 36 (2): 278–298.

Blaesi, H. R. 1987. “Lithostratigraphy and correlation of the Dogger sediments in the boreholes of Weiach, Riniken and Schafisheim.” http://inis.iaea.org/Search/search.aspx?orig_q=RN:19031494.

———. 1991. “Geology of the Potential Repository Site at Wellenberg.” *Nagra Bulletin (English Edition)* 1991 (1): 25–31.

Bossart, Paul. 2008. *Mont Terri Rock Laboratory Project: Programme 1996 to 2007 and Results*. Federal Office of Topography Swisstopo.

———. 2011. “Characteristics of the Opalinus Clay at Mont Terri.” *Mont Terri Project, Wabern Switzerland*. https://www.researchgate.net/profile/Paul_Bossart/publication/265227432_Characteristics_of_the_Opalinus_Clay_at_Mont_Terri/links/55d3046208ae7fb244f57452.pdf.

Bossart, Paul, Frédéric Bernier, Jens Birkholzer, Christophe Bruggeman, Peter Connolly, Sarah Dewonck, Masaaki Fukaya, Martin Herfort, Mark Jensen, and Jean-Michel Matray. 2018. “Mont Terri Rock Laboratory, 20 Years of Research: Introduction, Site Characteristics and Overview of Experiments.” In *Mont Terri Rock Laboratory, 20 Years*, 3–22. Springer.

Bossart, Paul, F. BURRUS, D. JAEGGI, and C. NUSSBAUM. 2017. “The Mont Terri Rock Laboratory.” In *Rock Mechanics and Engineering Volume 2*, 469–510. CRC Press.

Bossart, Paul, and Alan Geoffrey Milnes. 2017. *Mont Terri Rock Laboratory, 20 Years: Two Decades of Research and Experimentation on Claystones for Geological Disposal of Radioactive Waste*. Vol. 5. Birkhäuser.

Boulin, P. F., P. Bretonnier, N. Gland, and J. M. Lombard. 2012. “Contribution of the Steady State Method to Water Permeability Measurement in Very Low Permeability Porous Media.” *Oil & Gas Science and Technology – Revue d’IFP Energies Nouvelles* 67 (3): 387–401. https://doi.org/10.2516/ogst/2011169.

Boving, Thomas B., and Peter Grathwohl. 2001. “Tracer Diffusion Coefficients in Sedimentary Rocks: Correlation to Porosity and Hydraulic Conductivity.” *Journal of Contaminant Hydrology* 53 (1): 85–100.

Burkhalter, R. M., H. R. Bläsi, and S. Feist-Burkhardt. 1997. “Der Dogger \s s (Oberes Aalénien) in Den Bohrungen Herdern-1, Berlingen-1 Und Kreuzlingen-1 (Nordschweiz) Und Seine Beziehungen Zu Den Gleichaltrigen Schichten Im Nordjura.” *Eclogae Geologicae Helvetiae* 90: 269–291.

Burkhalter, Reto M. 1996. “Die Passwang-Alloformation (Unteres Aalénien Bis Unteres Bajocien) Im Zentralen Und Nördlichen Schweizer Jura.” *Eclogae Geologicae Helvetiae* 89 (3): 875–934.

Cey, Bradley D., S. L. Barbour, and M. Jim Hendry. 2001. “Osmotic Flow through a Cretaceous Clay in Southern Saskatchewan, Canada.” *Canadian Geotechnical Journal* 38 (5): 1025–1033.

Classics Brunauer, S., P. Emmett, and E. Teller. 1938. “Adsorption of Gases in Multimolecular Layers.” *Journal of the American Chemical Society* 60: 309–19.

Croisé, J., G. Mayer, P. Marschall, J. M. Matray, T. Tanaka, and P. Vogel. 2006. “Gas Threshold Pressure Test Performed at the Mont Terri Rock Laboratory (Switzerland): Experimental Data and Data Analysis.” *Oil & Gas Science and Technology - Revue de l’IFP* 61 (5): 631–45. https://doi.org/10.2516/ogst:2006003.

Cuss, Robert, Jon Harrington, Richard Giot, and Christophe Auvray. 2014. “Experimental Observations of Mechanical Dilation at the Onset of Gas Flow in Callovo-Oxfordian Claystone.” *Geological Society, London, Special Publications* 400 (1): 507–519.

Davy, Catherine, S. M’Jahad, F. Skoczylas, and J. Talandier. 2013. “Migration de Gaz Au Travers de l’argilite de Bure: Mise En Evidence d’un Passage Discontinu.” *Rencontres AUGC*.

Faulkner, D. R., and E. H. Rutter. 2000. “Comparisons of Water and Argon Permeability in Natural Clay-Bearing Fault Gouge under High Pressure at 20° C.” *Journal of Geophysical Research: Solid Earth* 105 (B7): 16415–16426.

Filomena, C. M., J. Hornung, and H. Stollhofen. 2014. “Assessing Accuracy of Gas-Driven Permeability Measurements: A Comparative Study of Diverse Hassler-Cell and Probe Permeameter Devices.” *Solid Earth* 5 (1): 1.

Gautschi, Andreas. 2001. “Hydrogeology of a Fractured Shale (Opalinus Clay): Implications for Deep Geological Disposal of Radioactive Wastes.” *Hydrogeology Journal* 9 (1): 97–107.

Heitzmann, P. 2004. “Mont Terri Project—Hydrogeological Synthesis, Osmotic Flow, Berichte Des BWG, Serie Geologie, No. 6.” Bern:[sn].

Jaeggi, David, Ben Laurich, Christophe Nussbaum, Kristof Schuster, and Peter Connolly. 2017. “Tectonic Structure of the ‘Main Fault’ in the Opalinus Clay, Mont Terri Rock Laboratory (Switzerland).” *Swiss Journal of Geosciences* 110 (1): 67–84.

Klinkenberg, L. J., and others. 1941. “The Permeability of Porous Media to Liquids and Gases.” In *Drilling and Production Practice*. American Petroleum Institute. https://www.onepetro.org/conference-paper/API-41-200.

Kostek, Sergio, Lawrence M. Schwartz, and David Linton Johnson. 1992. “Fluid Permeability in Porous Media: Comparison of Electrical Estimates with Hydrodynamical Calculations.” *Physical Review B* 45 (1): 186.

Letham, E. A., and R. M. Bustin. 2015. “Klinkenberg Gas Slippage Measurements as a Means for Shale Pore Structure Characterization.” *Geofluids*. http://onlinelibrary.wiley.com/doi/10.1111/gfl.12147/pdf.

Marschall, P., J. Croisé, L. Schlickenrieder, J. Y. Boisson, P. Vogel, and S. Yamamoto. 2004. “Synthesis of Hydrogeological Investigations at the Mont Terri Site (Phases 1 to 5).” *Mont Terri Project–Hydrogeological Synthesis, Osmotic Flow, Report of the Federal Office for Water and Geology (Bern, Switzerland). Geology Series* 6: 7–92.

Marschall, P., S. Horseman, and Thomas Gimmi. 2005. “Characterisation of Gas Transport Properties of the Opalinus Clay, a Potential Host Rock Formation for Radioactive Waste Disposal.” *Oil & Gas Science and Technology* 60 (1): 121–139.

McPhee, C. A., K. G. Arthur, and others. 1994. “Relative Permeability Measurements: An Inter-Laboratory Comparison.” In *European Petroleum Conference*. Society of Petroleum Engineers. https://www.onepetro.org/conference-paper/SPE-28826-MS.

Mercer, James W., George F. Pinder, and Ian G. Donaldson. 1975. “A Galerkin-Finite Element Analysis of the Hydrothermal System at Wairakei, New Zealand.” *Journal of Geophysical Research* 80 (17): 2608–2621.

Neuzil, C. E. 2000. “Osmotic Generation of ‘Anomalous’ Fluid Pressures in Geological Environments.” *Nature* 403 (6766): 182–184.

Nussbaum, Christophe, Paul Bossart, Florian Amann, and Charles Aubourg. 2011. “Analysis of Tectonic Structures and Excavation Induced Fractures in the Opalinus Clay, Mont Terri Underground Rock Laboratory (Switzerland).” *Swiss Journal of Geosciences* 104 (2): 187.

Pape, Hansgeorg, Christoph Clauser, and Joachim Iffland. 1999. “Permeability Prediction Based on Fractal Pore-Space Geometry.” *Geophysics* 64 (5): 1447–1460.

Pearson, F. J., D. Arcos, A. Bath, J. Y. Boisson, A. M. Fernández, H. E. Gaebler, E. Gaucher, et al. 2003. “Mont Terri Project-Geochemistry of Water in the Opalinus Clay Formation at the Mont Terri Rock Laboratory-Synthesis Report.” *Reports of the Swiss Federal Office for Water and Geology, Geology Series, No. 5, Bern, Switzerland.* 5. http://boris.unibe.ch/86639/.

Profice, Sandra. 2014. “Mesure de Propriétés Monophasiques de Milieux Poreux Peu Perméables Par Voie Instationnaire.” Université de Bordeaux. https://tel.archives-ouvertes.fr/tel-01127347/.

Schaeren, G., and J. Norbert. 1989. “Tunnels Du Mont Terri et Du Mont Russelin—La Traversée Des ‘Roches à Risques’; Marnes et Marnes à Anhydrite.” *Société Suisse Des Ingénieurs et Des Architectes, Documentation, SIA D* 37: 19–24.

Singh, Harpreet. 2016. “A Critical Review of Water Uptake by Shales.” *Journal of Natural Gas Science and Engineering* 34: 751–766.

Singh, Harpreet, and Jianchao Cai. 2019a. “A Feature-Based Stochastic Permeability of Shale: Part 1—Validation and Two-Phase Permeability in a Utica Shale Sample.” *Transport in Porous Media* 126 (3): 527–560.

———. 2019b. “Permeability of Fractured Shale and Two-Phase Relative Permeability in Fractures.” In *Petrophysical Characterization and Fluids Transport in Unconventional Reservoirs*, 105–132. Elsevier.

Takeda, M., T. Hiratsuka, M. Manaka, S. Finsterle, and K. Ito. 2014. “Experimental Examination of the Relationships among Chemico-Osmotic, Hydraulic, and Diffusion Parameters of Wakkanai Mudstones.” *Journal of Geophysical Research: Solid Earth* 119 (5): 4178–4201.

552 Thury, M., and P. Bossart. 1999. “The Mont Terri Rock Laboratory, a New International
553 Research Project in a Mesozoic Shale Formation, in Switzerland.” *Engineering Geology*
554 52 (3): 347–359.
555 Trémosa, Joachim. 2010. “Influence of Osmotic Processes on the Excess-Hydraulic Head
556 Measured in the Toarcian/Domerian Argillaceous Formation of Tournemire.”
557 https://inis.iaea.org/search/search.aspx?orig_q=RN:44128157.
558 Ullman, William J., and Robert C. Aller. 1982. “Diffusion Coefficients in Nearshore Marine
559 Sediments.” *Limnology and Oceanography* 27 (3): 552–556.
560 Van Loon, Luc R., and Jens Mibus. 2015. “A Modified Version of Archie’s Law to Estimate
561 Effective Diffusion Coefficients of Radionuclides in Argillaceous Rocks and Its
562 Application in Safety Analysis Studies.” *Applied Geochemistry* 59: 85–94.
563 Yu, Catherine, Jean-Michel Matray, Julio Gonçalvès, David Jaeggi, Werner Gräsle, Klaus
564 Wieczorek, Tobias Vogt, and Erik Sykes. 2017. “Comparative Study of Methods to
565 Estimate Hydraulic Parameters in the Hydraulically Undisturbed Opalinus Clay
566 (Switzerland).” *Swiss Journal of Geosciences* 110 (1): 85–104.
567

568 **Additionnal reference**

569 Marshall P., Croisé J., Schlickenrieder L., Boisson J.-Y., Vogel P., Yamamoto S. (2004)
570 Synthesis of hydrogeological investigations at the Mont Terri site. In Heitzmann, P. ed.
571 (2004): Mont Terri Project – Hydrogeological Synthesis, Osmotic Flow. Reports of the
572 Federal Office for Water and Geology (FOWG), Geology Series No. 6.
573

574 **Tables and Figures**

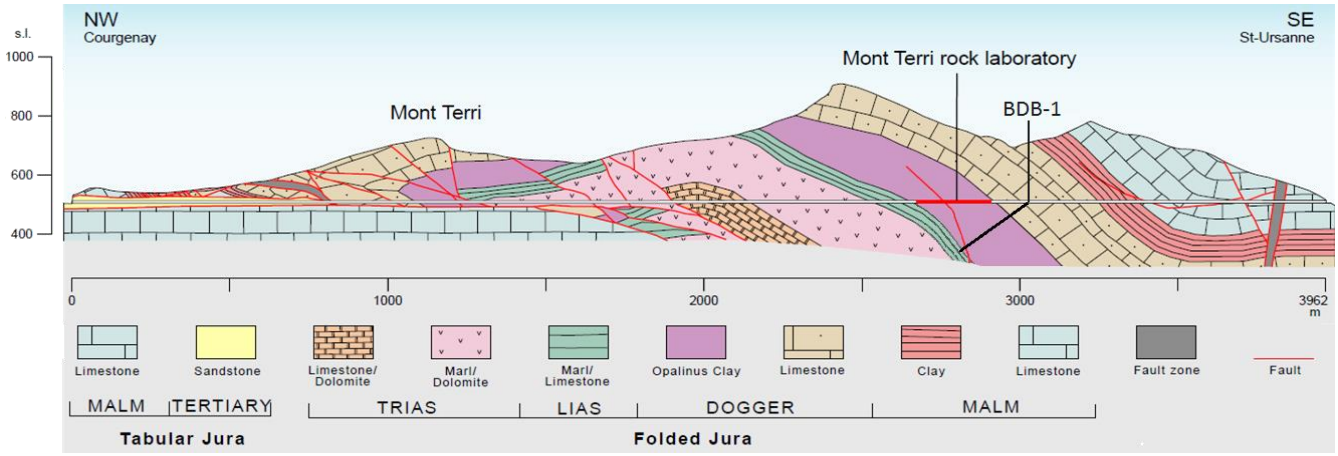

575

576 *Figure 1: Geological cross section of the Mont Terri anticline showing the Opalinus Clay formation,*
577 *tunnel gallery and the BDB-1 Borehole (modified from Freivogel et al., 2003)*

578
579

580

Formation	*Plug ID*	*Distance from borehole mouth (m)*	*Width (mm)*	*Length (mm)*	*Weight (g)*	*Orientation with respect of the stratification*	
OPA (Sandy)	**M12a***	**116.54**	**39.53**	**25.76**	**76.19**	⊥	
	M12b	**116.54**	**39.52**	**27.67**	**84.36**	⊥	
	M12c*	**116.54**	**39.6**	**55.08**	**171.8**		//
	M12d*	116.54	39.79	12.835	39.84		//
	M13a	**125.38**	**39.51**	**26.79**	**82.12**	⊥	
	M13b*	**125.38**	**39.6**	**42.16**	**127.2**		//
OPA (shaly)	M14a	136.58	39.56	7.58	21.37	⊥	
	M14b	136.58	39.52	12.22	36.73	⊥	
	M14c*	**136.58**	**39.5**	**30.23**	**92.52**		//
	M14d	136.58	39.805	4.975	14.12	⊥	
	M16a*	155.72	39.46	33.72	101.84		//
	M16b*	**155.72**	**39.65**	**29.39**	**89.8**	⊥	
OPA (shaly)	**M21a**	**204.98**	**39.78**	**12.29**	**36.97**	⊥	
	M21b*	204.98	14.155	20.555	7.62		//
	M22a	**213.48**	**39.49**	**7.34**	**20.96**	⊥	
	M22b*	213.48	39.52	39.73	118.37		//

581

582 *Table 1: Samples ID, distance from the borehole head, size, and orientation with respect to the*
583 *stratification (⊥: perpendicular and // : parallel). Asterisk mentions the samples covered with resin.*
584 *Black color is referred to samples with successful permeability results.*

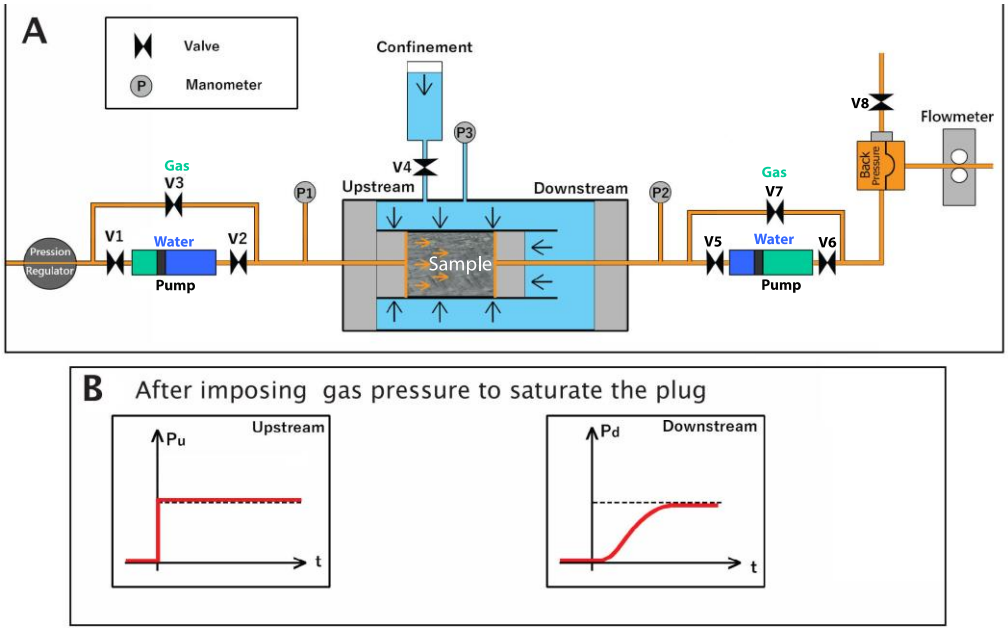

Figure 2: A) Hassler cell containing a clay sample. P1, P2, and P3 are manometers measuring the upstream, downstream, and confining pressures, respectively. V1 to V8 are valves. Two pumps are used to ensure water permeability measurements. B) Saturation step of the sample: applying a pressure on the upstream side and waiting to be achieved on the downstream one.

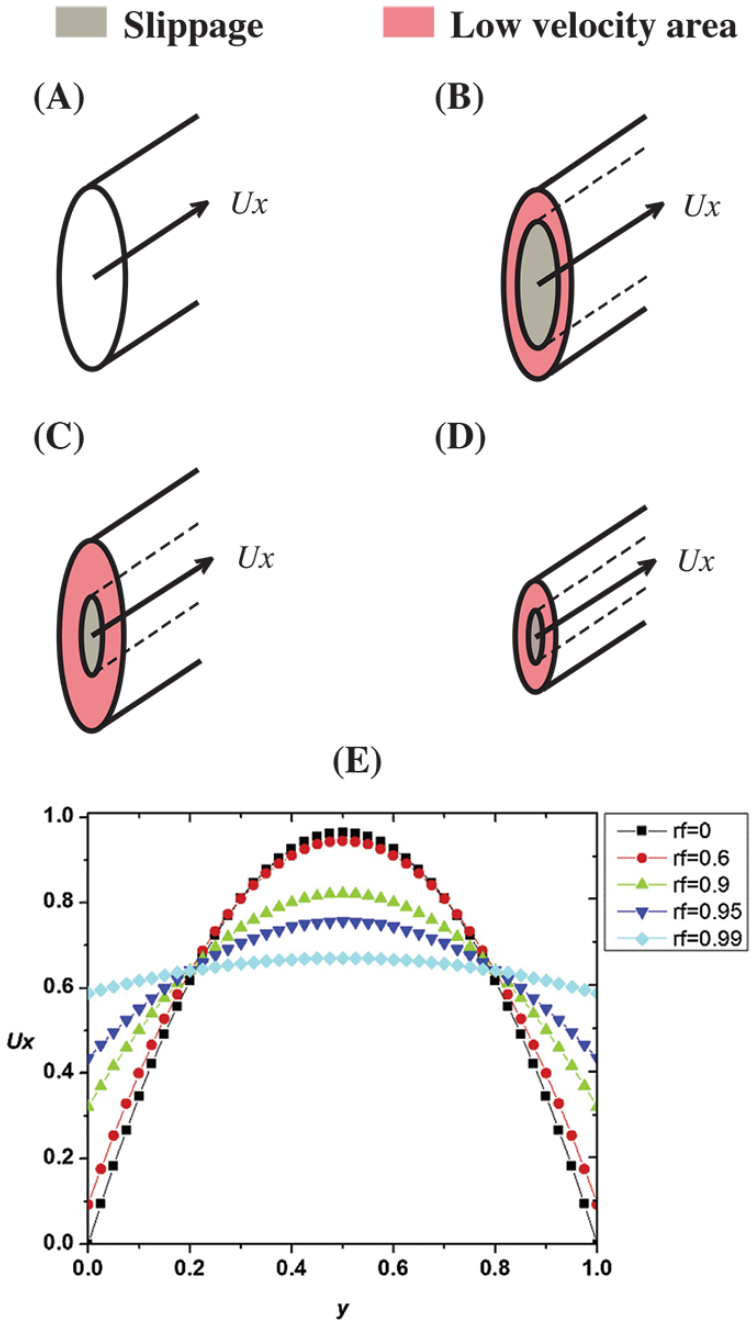

Figure 3: Slippage effect controlled by the mean free path of the gas (A,B,C) and capillary size (D) (modified from Letham et al. 2015 and Arabjamaloei and Ruth 2016).red color represents low velocity areas and grey color represent the slippage effect A) At very high imposed pressure, the mean free path of the gas is small resulting in zero slippage at the pore wall. Moreover, the reflection coefficient "rf" acting in the same way as the imposed pressure is high, resulting in a high velocity at the pore walls due to its high value as shown in (E) (see the example of rf=0.99). B) When the imposed pressure decreases, the "rf" and the velocity at the pore walls decreases too, resulting in a larger mean free path of the gas and the onset of slippage effect. C), The imposed pressure continue to decrease in addition to the "rf" and the velocity at the pore walls. In such conditions, the mean free path increase and the slippage effect become larger. D) In (B) and (C) the capillary size remain constant but changes in (D). When the capillary size decrease, and for the same imposed conditions as in (B), slippage effect appears greater comparing to the capillary size.(E) figure E represents the velocity versus pore diameter, the increase in rf value leads to the increase of the velocity at the pore walls.

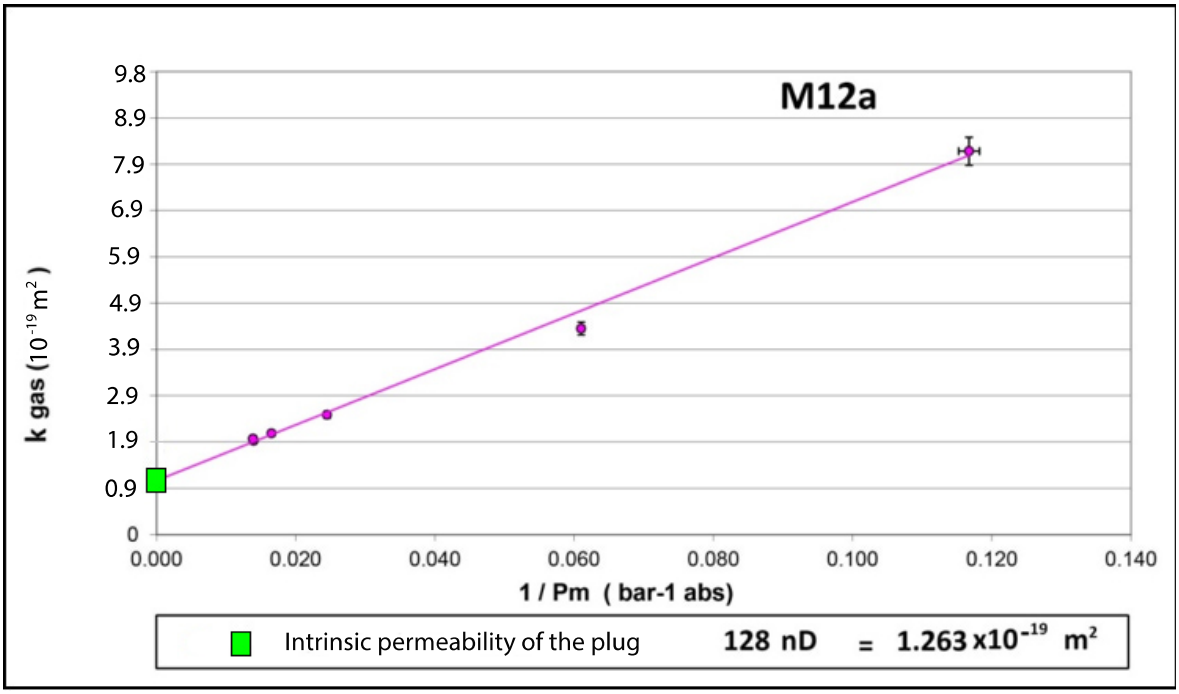

Figure 4: Permeability values (k gas) vs. inverse of the mean pressure for the sample M12a

607

Sample ID	12	13	14	16	21	22
	mg/L	mg/L	mg/L	mg/L	mg/L	mg/L
Na^{+}	738.22	4926.4	7209.8	12278	12337	10686
K^{+}	16.34	191.6	262.6	143.98	305.43	387.24
Mg^{2+}	94.14	1197.4	1808.6	636.16	3073.7	3055
Ca^{2+}	328.53	3948.3	5422.4	2564.1	4920.7	4588.8
Sr^{2+}	15.75	165.93	208.32	80.36	136.63	141.55
Cl^{-}	567.25	6097.9	8898.7	8650.9	12196	11097
SO_4^{2-}	120.16	844.15	931.14	1892.5	1767.9	1594.1
Total	1880.4	17371	24741	26246	34738	31549

608 *Table 2: Chemical composition of water for permeability measurements*

609

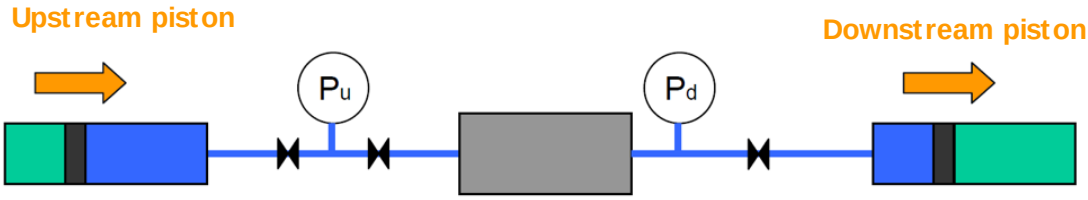

Figure 5: Schematic representation of the dual piston pumps used in water permeability measurement. In the steady state method, water is injected using a "Push-Pull" dual piston pump. Blue colour in the pumps represents water and green colour represents gas. The gray rectangle represents the sample.

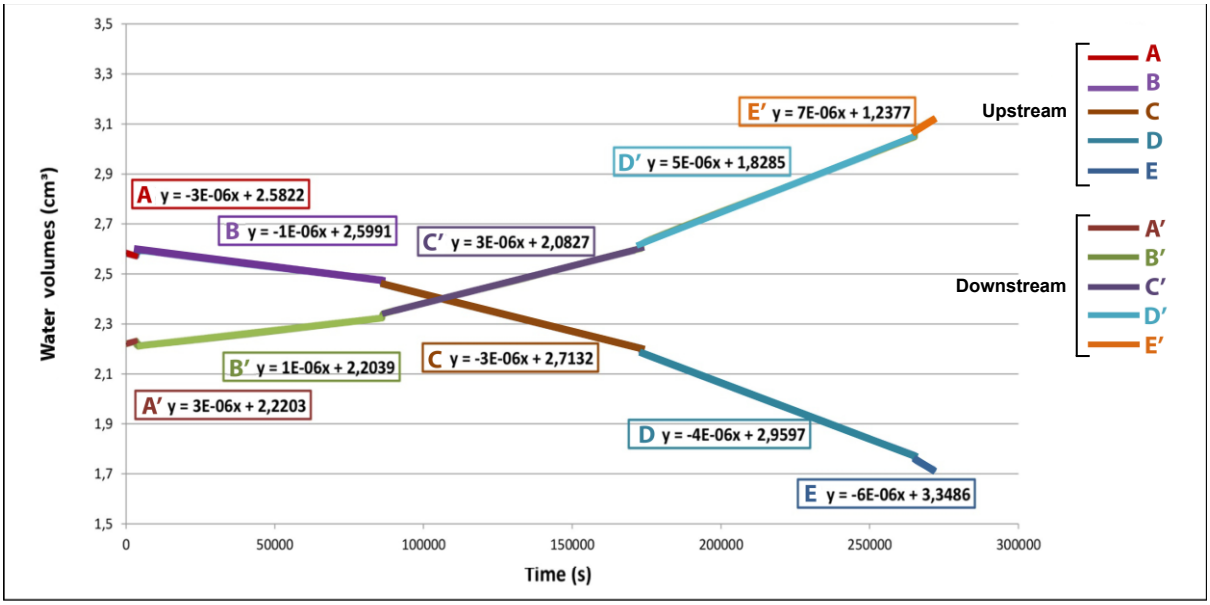

Figure 6: Variation of the volume of water vs. time in the upstream and downstream side of the Hassler cell. A Trendline equation is calculated for each pressure gradient imposed during the measurement.

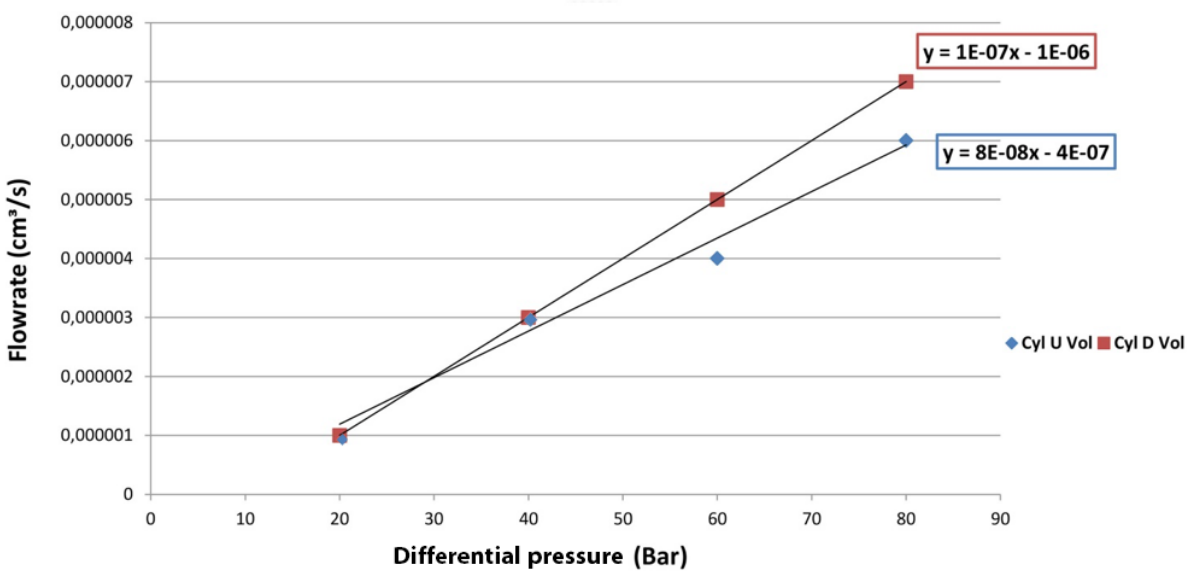

Figure 7: Water flowrate vs. differential pressure in the upstream and downstream sides. Upstream pressure is measured by manometer P1 and downstream pressure is measured by manometer P2.

Formation	Plug ID	Distance from borehole mouth	Gas permeability measurements on ^plugs		Gas permeability measurements on // plugs		Water permeability measurements on // plugs		covered with resin
		m	m^2	m^2	m^2	m^2	m^2	m^2	
			Results	Errors	Results	Errors	Results	Errors	
OPA (Sandy)	M12a	116.54	1.26E-19	1.25E-31					Yes
	M12b	116.54	7.70E-20	7.60E-32					No
	M12c	116.54					1.38E-20	1.90E-22	Yes
	M12d	116.54							Yes
	M13a	125.38	2.31E-19	2.28E-31					No
	M13b	125.38			2.58E-20	2.55E-32			Yes
	M13c	125.38							Yes
OPA (shaly)	M14a	136.58							No
	M14b	136.58							No
	M14c	136.58			2.96E-20	2.92E-32			Yes
	M14d	136.58							No
	M16a	155.72							Yes
	M16b	155.72	1.30E-20	5.28E-31					Yes
OPA (shaly)	M21a	204.98	4.737E-20	4.68E-32					No
	M21b	204.98							Yes
	M22a	213.48	6.908E-21	6.82E-33					No
	M22b	213.48							Yes

Table 3: Successful saturated gas and water permeability on plugs ⊥ and // to the bedding (uncertainty calculation is available in the SI).

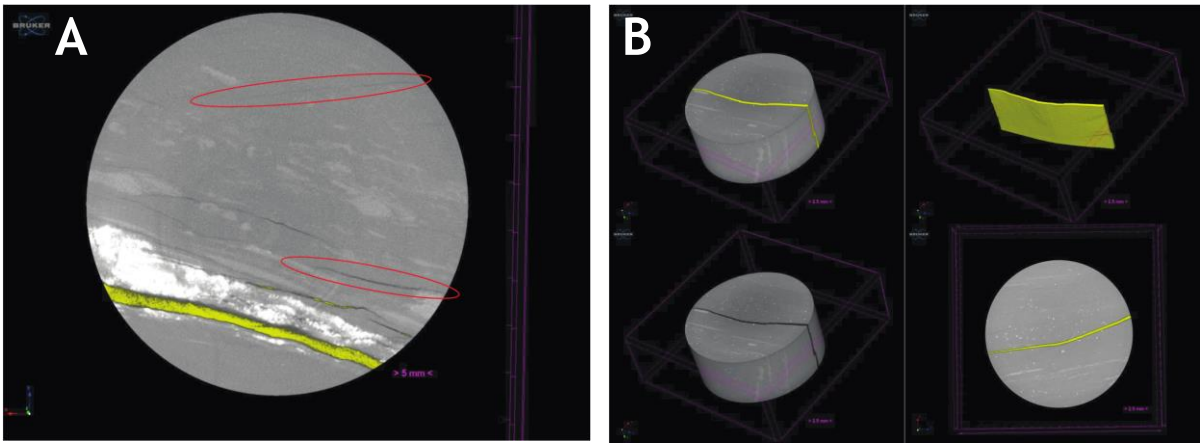

Figure 8: Micro-computed tomography on two samples, yellow colour represents epoxy resin: A) sample M12D shows major cracks filled with resin in yellow,and minor cracks surrounded with red ellipses hard to analyse due to voxel resolution. This sample provided a non-satisfactory permeability result, B) sample M14c shows a single crack filled with epoxy resin in yellow and provided a satisfactory permeability result.

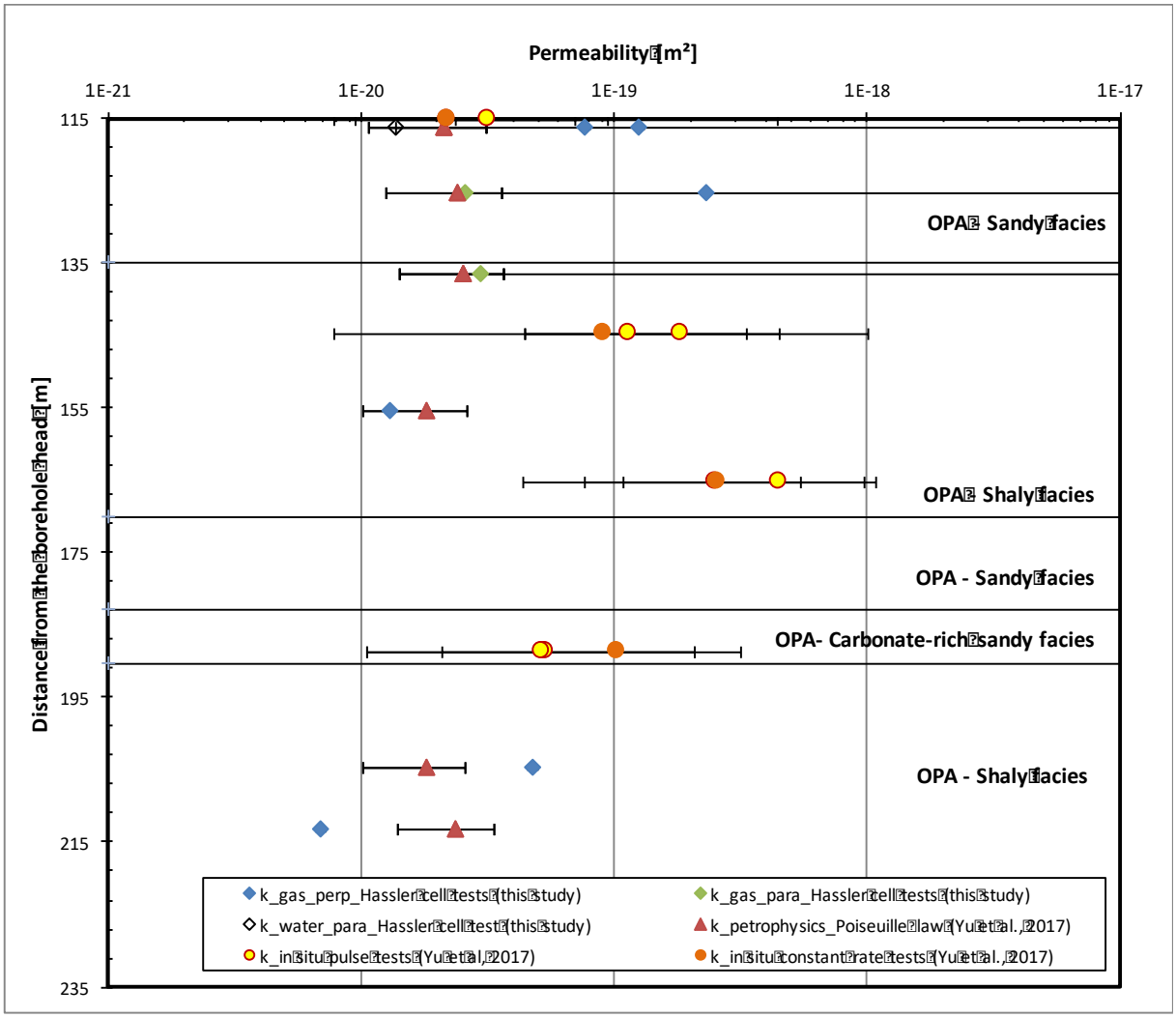

Figure 9: Comparison of water and gas permeability results obtained at laboratory scale from Hassler cells (parallel or perpendicular to bedding) and petrophysical measurements to in situ hydraulic tests as a function of the distance from the borehole head. Errors on Hassler Cell results are minor and do not appear in the graph.

644
645

	Hassler cell	Poiseuille-type law method	In situ tests	
			Constant rate	Pulse
Mean permeability value for the sandy facies (m^2)	$1.15.10^{-19}$	$2.26.10^{-20}$	$2.2.10^{-20}$	$3.2.10^{-20}$
Mean permeability value for the shaly facies (m^2)	$2.4.10^{-20}$	$2.07.10^{-20}$	$1.7.10^{-19}$	$2.5.10^{-19}$

646 *Table 4: Comparison of mean permeability results acquired using three different methods for the*
647 *Opalinus*

648

Figure captions:

Figure 1: Geological cross section of the Mont Terri anticline showing the Opalinus Clay formation, tunnel gallery and the BDB-1 Borehole (modified from Freivogel et al., 2003)

Figure 2: A) Hassler cell containing a clay sample. P1, P2, and P3 are manometers measuring the upstream, downstream, and confining pressures, respectively. V1 to V8 are valves. Two pumps are used to ensure water permeability measurements. B) Saturation step of the sample: applying a pressure on the upstream side and waiting to be achieved on the downstream one.

Figure 3: Slippage effect controlled by the mean free path of the gas (A,B,C) and capillary size (D) (modified from Letham et al. 2015 and Arabjamaloei and Ruth 2016). A) At very high imposed pressure, the mean free path of the gas is small as they act in the opposite way resulting in zero slippage at the pore wall. Moreover, the "rf" acting in the same way as the imposed pressure is high, resulting in a high velocity at the pore walls due to its high value as shown in (E). B) When the imposed pressure decreases, the "rf" and the velocity at the pore walls decreases too, resulting in a larger mean free path of the gas and the onset of slippage effect at the pore walls. C), The imposed pressure continue to decrease in addition to the "rf" and the velocity at the pore walls. In such conditions, the mean free path increase and the slippage effect become larger. D) In (B) and (C) the capillary size remain constant but changes in (D). When the capillary size decrease, and for the same imposed conditions as in (B), slippage effect appears greater comparing to the capillary size.

Figure 4: Permeability values (k gas) vs. inverse of the mean pressure for the sample M12a

Figure 5: Schematic representation of the dual piston pumps used in water permeability measurement. In the steady state method, water is injected using a "Push-Pull" dual piston pump. Blue colour in the pumps represents water and green colour represents gas. The gray rectangle represents the sample.

Figure 6: Variation of the volume of water vs. time in the upstream and downstream side of the Hassler cell. A Trendline equation is calculated for each pressure gradient imposed during the measurement.

Figure 7: Water flowrate vs. differential pressure in the upstream and downstream sides. Upstream pressure is measured by manometer P1 and downstream pressure is measured by manometer P2.

Figure 8: Micro-computed tomography on two samples, yellow colour represents epoxy resin: A) sample M12D shows major cracks filled with resin in yellow,and minor cracks surrounded with red ellipses hard to analyse due to voxel resolution. This sample provided a non-satisfactory permeability result, B) sample M14c shows a single crack filled with epoxy resin in yellow and provided a satisfactory permeability result.

Figure 9: Comparison of water and gas permeability results obtained at laboratory scale from Hassler cells (parallel or perpendicular to bedding) and petrophysical measurements to in situ hydraulic tests as a function of the distance from the borehole head. Errors on Hassler Cell results are minor and do not appear in the graph.

692
693 **Table caption**

694 Table 1: Samples ID, distance from the borehole head, size, and orientation with respect to the
695 stratification (⊥: perpendicular and // : parallel). Asterisk mentions the samples covered
696 with resin. Black color is referred to samples with successful permeability results.
697 Table 2: Chemical composition of water for permeability measurements
698 Table 3: Successful saturated gas and water permeability on plugs ⊥ and // to the bedding
699 (uncertainty calculation is available in the SI).
700 Table 4: Comparison of mean permeability results acquired using three different methods for
701 the Opalinus
702